Proc. IEEE Int. Conf. on Multisensor Fusion and Integration in Intelligent Systems (MFI-2008), pp. 526-532, Seoul, Korea, Aug. 2008.

Simultaneous Estimation of Road Region and Ego-Motion with Multiple Road Models

Yoshiteru Matsushita
Department of Mechanical Engineering,
Osaka University
matsushita@cv.mech.eng.osaka-u.ac.jp

Jun Miura
Department of Information
and Computer Sciences,
Toyohashi University of Technology
jun@ics.tut.ac.jp

***Abstract*— This paper describes a method of simultaneously estimating the road region and the ego-motion for outdoor mobile robots. Temporal integration of sensor data is effective for robust estimation of road region. To integrate sensor data obtained at multiple places, the robot's ego-motion has to be estimated simultaneously. It is also necessary to use multiple sensors for reliable estimation because road boundary features from one sensor, such as white lines and curbs, are not always available. In addition, to cope with the change of the road type, we prepare multiple road models for estimation. We implement this multi sensor-based, simultaneous estimation of road region and ego-motion using a particle filter. We also devise a technique for generating new particles to cope with gradual road type changes. The proposed method has been successfully applied to autonomous navigation in various road scenes. Application to other types of roads such as intersections is also discussed.**

I. Introduction

Research on ITS (Intelligent Transportation Systems) has recently been active. One of the objectives of ITS research is to realize safe driving by, for example, driver assistance systems like lane departure warning. Development of autonomous robots like guide robots has also been widely conducted. These systems require an ability to recognize traversable regions such as road regions.

GPS systems, combined with an accurate map, can provide location information. But for safe driving, local information on the road region such as curbs, road and lane boundary lines, and road shoulders, should be utilized, and such information can only be obtained on-site. It is, therefore, necessary to estimate road regions using external sensors such as vision and range finders.

Many works use vision for detecting road boundaries [1], [2], but such boundaries are not always easily detectable. Others use range finders to detect road boundaries from their shape information. If we use a 2D scanning range fingers, guardrails or clear curbs should exist [3], [4], [5].

Road region detection only from the latest observation is vulnerable to occasional sensing failures or missing of features, such as shadows in the image or discontinuity of curbs. It is, therefore, necessary to temporally integrate sensor data for reliable detection.

Wijesoma et al. [3] developed a method of detecting and estimating road boundary from a sequence of curb positions detected by a laser range finder looking slightly downwards. They estimated road boundary parameters using Kalman filter. This method assumes that curb positions on both sides are obtained clearly from the laser data and the vehicle motion is correct. Kirchner and Heinrich [4] proposed a method of estimating road boundary parameters using a sequence of horizontal laser-scanned data. They used a 3rd order polynomial boundary model as an approximation of clothoid curves, and estimated its parameters using Kalman filter. They estimated only road boundary parameters by assuming a correct vehicle motion. In addition, since they use horizontal scanned data, some objects (e.g., guardrails) should exist at the roadside along the road. Cramer and Wanielik [5] proposed a similar method of estimating road boundary parameters.

Since an accurate ego-motion estimation only from internal sensors (i.e., dead reckoning) is difficult, it is necessary to estimate the ego-motion as well as the road region using external sensors. There are various road scenes and, therefore, appropriate features to estimate the road region may be different from place to place. For example, curbs may be removed at the entrance of shops; lanes are sometimes almost erased in an old road; unpaved roads may be detected by using only color differences between the road region and the roadside region. We, therefore, use multiple sensors and features to estimate the road region robustly.

Some previous works have used multiple sensors for navigation. Langer and Jochem [6] performed a fusion of radar and vision data for detecting roadway obstacles. Miura et al. [7] developed a method of reliable free space detection by integrating an omni-directional stereo and a laser range finder. However, the purpose of these works is not road region detection but obstacle detection.

This paper deals with simultaneous estimation of road region and ego-motion using vision and laser range data. We implement the estimation method using a particle filter. To cope with a gradual change of road type, we prepare multiple road models and devise a technique for generating new particles corresponding to such multiple models.

The rest of the paper is organized as follows. Sec.II presents a system overview. Sec. III defines the road models and the state vector. Sec. IV explains the processing of range and image data and the calculation of likelihood of a state. Sec. V explains the particle filter-based data integration and the model generation. Sec. VI presents experimental results of the method for various road scenes. Sec.VII summarizes

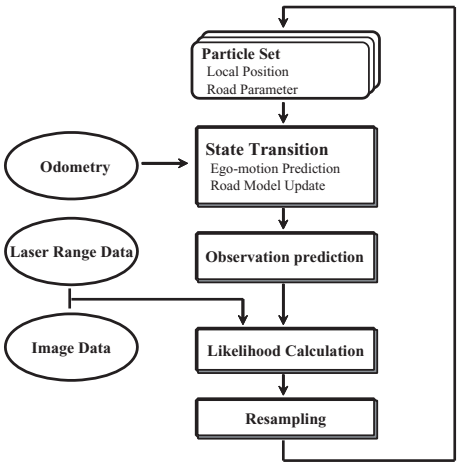

Fig. 1. System overview.

the paper and discusses future work.

II. System Overview

Fig. 1 shows an overview of the system. After each iteration, a set of particles is kept in the system. Each particle contains a robot pose and the parameters of a road model with respect to the current origin. The state transition step performs the following two operations. One is the coordinate transformation using an estimated ego-motion by odometry. The other is road model generation based on the prediction of possible road type changes. The observation prediction step calculates what observation will be obtained from the robot position and the road parameters. The likelihood calculation step processes range and image data to extract features and calculates the likelihood of each particle from such features and the predicted observation for the particle. The final step is the resampling.

III. Road Models and State Vectors

Two-dimensional shape of the road can be classified roughly into straight lines and curves. Usually a clothoid curve, whose curvature changes smoothly, is used in the connected part of a straight line and a curve. Since the objective of the method is not estimating an accurate road shape but get an estimate which is sufficient for safe and efficient autonomous driving, we use only straight lines and circles as the models of road shape.

We connect two consecutive road models so that their tangents coincide with each other at the connection point. To avoid a frequent switch of road models due to errors in observations, we switch the road model, if necessary, only when the robot advances by a certain distance. Currently we set the distance to $10\,[m]$; this is the same as the maximum observation range. When the robot crosses a potential model-switching point, the new road models are generated (See Sec. V for the details).

For a simultaneous estimation of ego-motion and road region, the state vector includes parameters for both. The elements of the state vector are represented with respect to

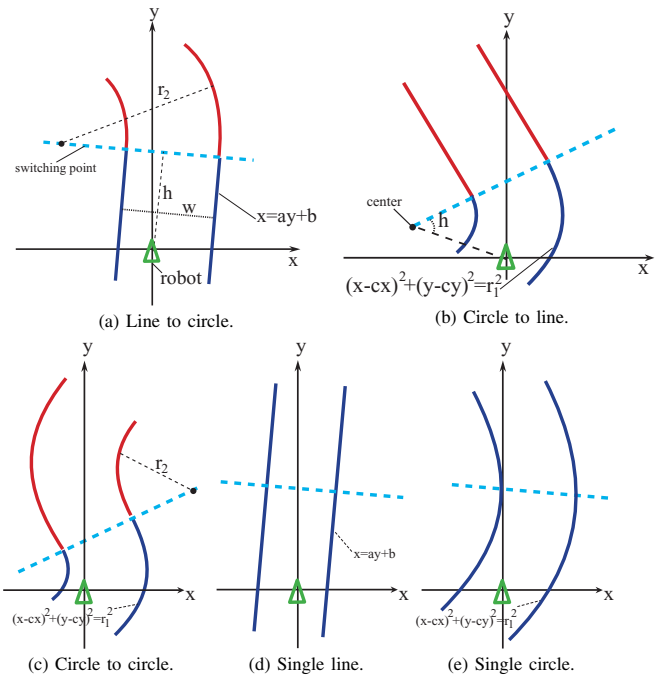

(a) Line to circle. (b) Circle to line.
(c) Circle to circle. (d) Single line. (e) Single circle.

Fig. 2. Road models.

the local origin, which is defined by the pose at the previous time step. The origin is updated in the state transition step in Fig. 1.

The robot pose is represented by its 2D position, x, y and orientation, d. Concerning the road parameters, we use the gradient and the intercept for representing straight lines, and the center position and the radius for circles. Road parameters are divided into the front part before the switching point and the rear part beyond the point. We also use w and h as the road width and the distance to the switching point, respectively. Fig. 2 shows five road models used in this paper. Road boundaries may sometimes be detected at different positions in range and image data. In such a case, the boundary for range data usually exists outside the one for image data (see Fig. 3, for example). So we explicitly represent and estimate the gap between the boundaries, both on the right and the left side of the road.

IV. Image and Range Data Processing for Likelihood Calculation

This section explains how to calculate the likelihood of each particle given a set of image and range data. We do not explicitly extract road boundaries but derive likelihood functions to be used for the calculation.

A. Range Data Processing

We use a SICK laser range finder (LRF). The LRF is set at the height of $0.45\,[m]$ looking downward by 5 degrees (see Fig. 4). Let h and ϕ be the height and the depression angle of LRF, and let l and α be the distance and the direction of a data point on the laser scanning plane. Then the position

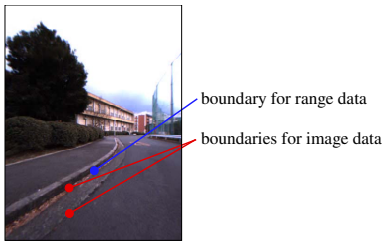

Fig. 3. Gap of road boundaries for range and image data.

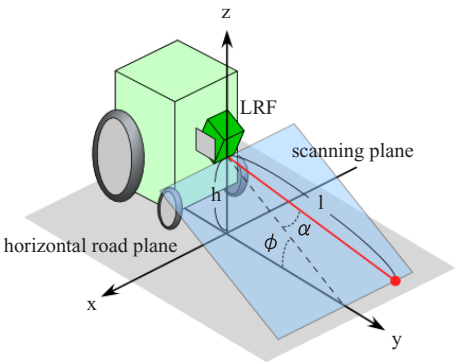

Fig. 4. Placement of laser range finder.

(x, y, z) of that point is given by:

$$x = l \sin \alpha, \quad (1)$$

$$y = l \cos \alpha \cos \phi, \quad (2)$$

$$z = h - l \cos \alpha \sin \phi. \quad (3)$$

At a curb position, a range data set has an L-shape but the data points are connected. The connectivity of data points are judged if the distance between a consecutive pair of data points is less than $1\,[m]$. A set of connected data points including the central one is analyzed to find L-shapes. We calculate the angle at each point from the two sets of the five neighboring points on both sides. A likelihood function of the angle, which assesses how likely a point is on the curb position, is then defined with a Gaussian; its mean and standard deviation are set to $90\,[deg]$ and $30\,[deg]$, respectively.

L-shape features may appear at places other than curb positions; for example, such a feature exists at the boundary of a pavement and a building wall. To exclude such spurious road boundaries, we use height information. We suppose that the robot is on a horizontal road plane, as shown in Fig. 4. In actual road scenes, however, since the gradient of the road can change, we consider the effect of such a change by considering the distribution of possible y positions (in the forward direction) of the road surface in the LRF data. The distribution is modeled as a Gaussian, whose mean and standard deviation are set to $h/\tan\phi = 5.1\,[m]$ and $3\,[m]$, respectively.

We discretize the range of the horizontal position x with $0.1\,[m]$ intervals. For each interval, we calculate the products

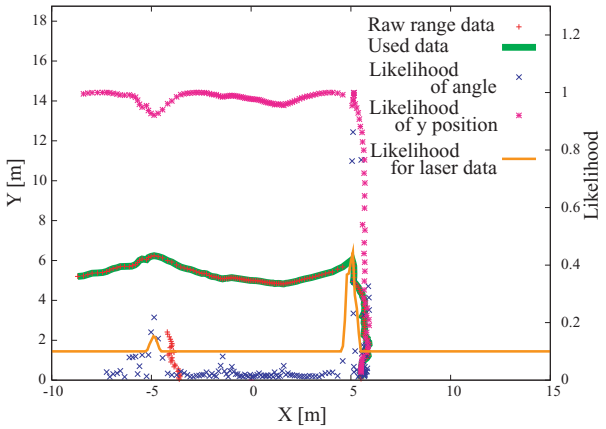

Fig. 5. LRF data and calculated likelihood values.

of the two likelihood values for data points in the interval, and take the maximum product as the likelihood for that interval. For an interval with no data, we calculate the likelihood by linear interpolation. Fig. 5 shows an example of likelihood calculation of the intervals.

We use this distribution of likelihood values to calculate the likelihood of each particle (i.e., each state vector). From the robot position and the road parameters of a particle, we can calculate the horizontal positions of road boundaries, which are actually the intersections of the laser scanning plane and the right and the left road boundary. The likelihood of the particle for laser data is then given by the product of the likelihood values at both horizontal positions.

B. Image Processing

We use a LadyBug2 (Pointgrey Research Inc.) omnidirectional camera system. This system has 5 CCD cameras, two of which are used in this research to cover the field of view of about $144\,[deg]$. We capture a pair of 512×384 images. We use two visual cues: road boundary lines and the boundaries between road and roadside regions. We use the intensity gradient images for the first cue and the color gradient images for the second one. The magnitude of gradient for each cue corresponds to the likelihood of the road boundary.

An intensity gradient image is obtained by applying a series of 3×3 median filter, a sobel filter, and a 11×11 smoothing filter. Fig. 6(b) shows the magnitude-of-gradient image obtained from the input image shown in Fig. 6(a).

Color gradient images are calculated as follows. We use the CIE L*a*b* color space, which fits well with the human perception. We model the color of a road surface with a Gaussian in the 2D color space and estimate it on-line. We sample color data in the estimated road region from the latest five frames, 100 samples from each frame. Using the estimated Gaussians, we make the image whose pixel values indicate how likely each pixel belongs to the road regions (see Fig. 6(c)). From this images, we calculate the color gradient of a pixel from the four regions of 15×7 pixels around that pixel (see Fig. 7). Let C_i be the averaged value of region i. At the left boundaries, since the gradient is

(a) Input image.

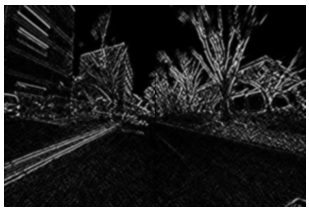

(b) Intensity gradient image.

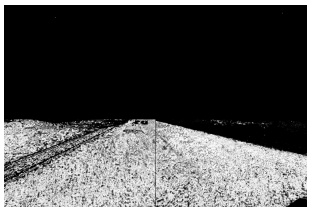

(c) Likelihood by color.

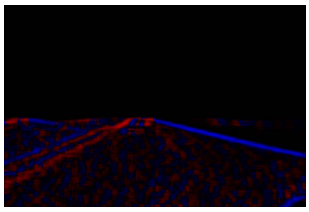

(d) Color gradient image.

Fig. 6. Calculation of intensity and color gradient.

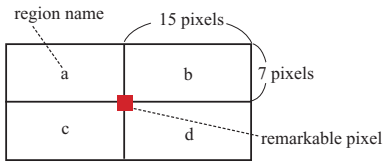

Fig. 7. Extraction of the color gradient.

rightward, we calculate the magnitude of gradient as:

$$\max(C_b - C_a, C_b - C_c, C_d - C_a, C_d - C_c). \quad (4)$$

The magnitude of gradient for the right boundaries is calculated similarly. Fig.6(d) shows the gradient image of road boundaries (red: left, blue: right).

The likelihood of a particle for image data is calculated as follows. Road boundary points in the image coordinates can be calculated from the road parameters and the robot pose of the particle. The averaged value m of the magnitude on these points is then calculated and input to the following sigmoid function to calculate the likelihood:

$$l(m) = \frac{1}{1 + \exp(-k(m - m_c))}, \quad (5)$$

where k and m_c are experimentally determined parameters.

V. A Particle Filter-Based Estimation Algorithm

A. State Transition

1) Ego-motion prediction: This step performs the coordinate transformation (see Sec. II) using odometry data and perturbs the robot pose part of each particle with an estimated odometry error. We currently use a very approximate error estimate; for a one meter movement, we use the standard deviations of $0.1\,[m]$, $0.1\,[m]$, and $0.1\,[rad]$ for x, y, and d, respectively. These values are set to proportional to the moving distance.

2) Road Model Update: As we stated in Sec. II, we switch the road model only when the robot advances by $10\,[m]$, and when the robot crosses a potential model-switching point, the new road models are generated. Each road model has two parts, the front and the rear part (see Sec. III). When the robot crosses a model-switching point, the rear part of the current model is transferred to the front part of a new model and a new rear part is attached. Since we cannot know in advance what type of road appears in the rear part, we generate all of the following as the rear road type: the line and a set of circles. The curvatures of circles are limited to $1/r = 0.02, 0.04, 0.06, 0.08, 0.10\,[1/m]$. For a particle which is judged to cross the switching point, multiple descendant particles are generated corresponding to various read road types. The weight w_{update} of a newly generated particle is set to $1/n_{new}$, the inverse of the number of newly generated particles. For a particle which is not judged to cross, the weight is one.

3) Road parameter prediction: In Sec. III, we defined road parameters. Among them, a road width and a gap between boundaries from range and image data may change as the robot moves. In addition, since we generate circular road models at the rear road part with a limited set of curvatures, as described above, we need to gradually adjust the curvature to the observation. We therefore estimate online the width, the gap, and the curvature, and fix the other road parameters for each particle.

B. Likelihood Calculation

The weight of each particle is calculated by the weight determined in the state transition and the likelihood values for range and image data.

The likelihood values may become very small due to a discontinuity of curb or cast shadows. Such a value makes the weight of a particle very small and that particle will most likely be deleted. To avoid this, we detect outliers using the likelihood value for each sensor at each side. If the maximum likelihood value for four combinations of the sensor and the side is less than a threshold (currently, 0.3), the particle under consideration is judged as an outlier and is deleted. The final weight w_{model} for an inlier particle is given by the product of the likelihood values l_{image} and l_{LRF} for image and range data and the weight w_{update} determined at the update step, that is,

$$w_{model} = (l_{image} \cdot l_{LRF}) \cdot w_{update}. \quad (6)$$

After calculating the weights, we perform a usual resampling step.

VI. Experimental Result

This section describes the experimental results conducted at two locations in our campus (See Fig.8). The first location is on a straight road partially with curbs. The second one is on a curved road with cast shadows.

(a) First experiment. (b) Second experiment.

Fig. 8. Location of the experiments.

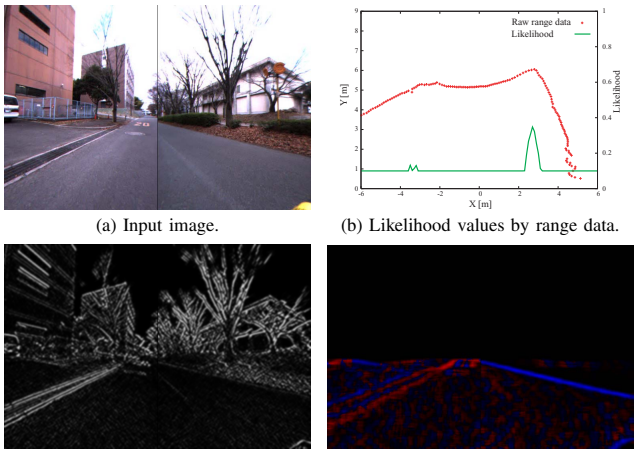

(a) Input image. (b) Likelihood values by range data.

(c) Intensity gradient image. (d) Color gradient image.

Fig. 9. Observation at step 55.

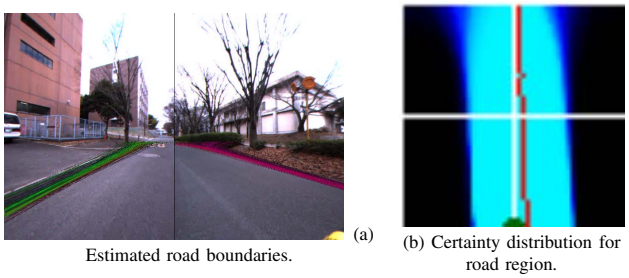

Estimated road boundaries. (a) (b) Certainty distribution for road region.

Fig. 10. Estimation result at step 55.

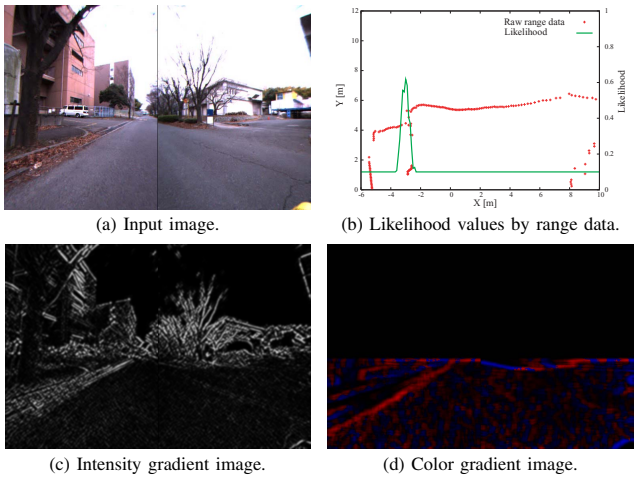

(a) Input image. (b) Likelihood values by range data.

(c) Intensity gradient image. (d) Color gradient image.

Fig. 11. Observation at step 40.

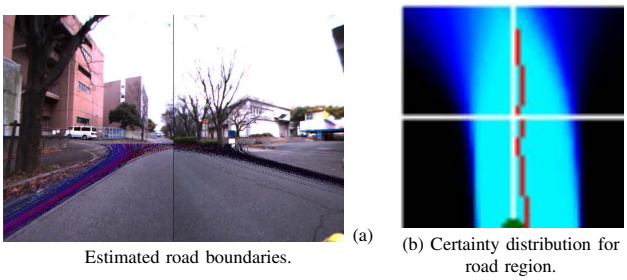

Estimated road boundaries. (a) (b) Certainty distribution for road region.

Fig. 12. Estimation result at step 40.

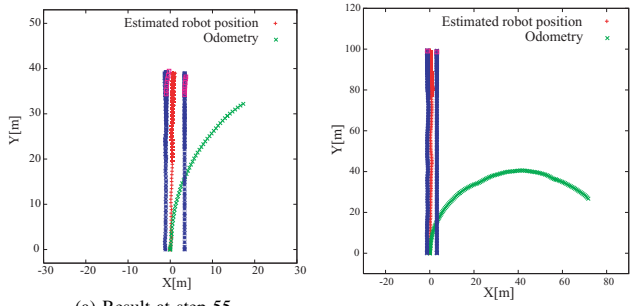

(a) Result at step 55. (b) Result at the final step.

Fig. 13. Estimation results of global road shape.

A. *Straight Road*

Fig. 8(a) shows the location of the first experiment. We manually moved the robot along the road and obtained 130 sets of range, image, and odometry data. The data are processed off-line with the number of particles being 500. At first there are curbs on both sides, but as the robot moves, there appears a parking space on the left (see Fig. 9(a)). At the entrance of the space, there are no curbs and, in this case, LRF data are not effective for detecting the left road boundary (see Fig. 9(b)). The right road boundary is, on the other hand, clearly detectable. If we have information on curb position at least on one side, we can estimate the road parameters by using predicted road models. Image data are also effective in this case, as shown in Fig. 9(c),(d). By integrating multiple information from both sensors, we can robustly estimate the road region. Fig. 10 shows the estimation result when the data shown in Fig. 9 was obtained at step 55. The left figure superimposes the road boundaries obtained from the particles after resampling on the input image. We assign the three primary colors to represent the likelihood of each piece of information as follows:

- R: likelihood using color gradient,
- G: likelihood using intensity gradient,
- B: likelihood using range data.

So for example, a purple line indicate that information of color gradient and range data supports the line. Fig. 10(b) shows a kind of certainty distribution of road regions, obtained from the current set of particles, in the robot local coordindates (the green semicircle is the robot); brighter

(a) Input image.

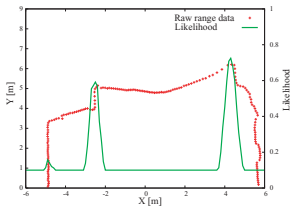

(b) Likelihood values by range data.

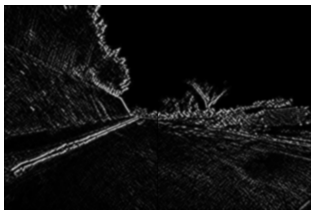

(c) Intensity gradient image.

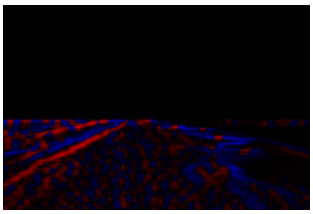

(d) Color gradient image.

Fig. 14. Observation at step 38.

(a)Input image.

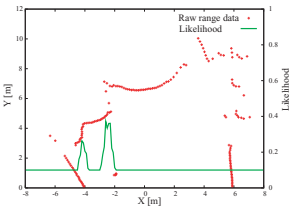

(b) Likelihood values by range data.

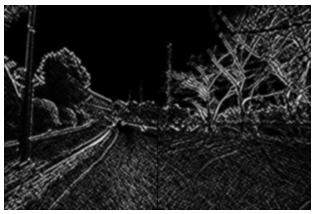

(c) Intensity gradient image.

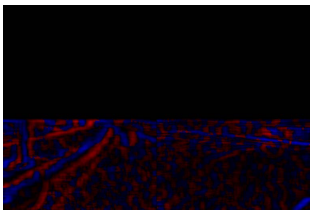

(d) Color gradient image.

Fig. 16. Observation at step 94.

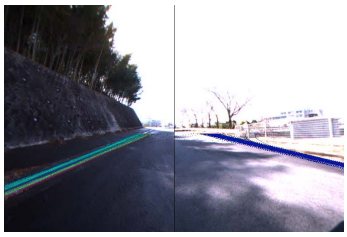

(a) Estimated road boundaries.

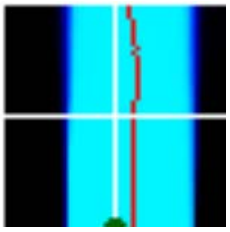

(b) Certainty distribution for road region.

Fig. 15. Estimation result at step 38.

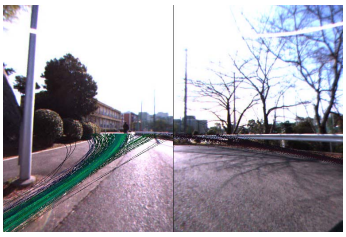

(a) Estimated road boundaries.

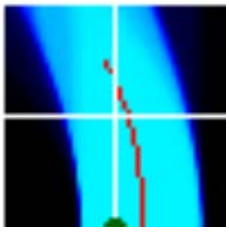

(b) Certainty distribution for road region.

Fig. 17. Estimation result at step 94

pixels indicate higher certainties. The center position of the road is also shown in red, which could be a guide for controlling the robot motion.

Figs. 11 and 12 are the input image, range and gradient information, and the estimation result at step 40. Cues on the right side are undetectable due to a branch. On the left side, a curb gradually moves outside towards a parking space, so many left curves survive as the estimated road boundaries. A few steps later, however, a left boundary for the intensity gradient become clearly detectable, and only straight line road models survive (see Fig. 10).

Each particle is split into a set of decendant particles at the road model update step, and a limited number of particles survive after the resampling. By tracing back from the current set of particles, we can obtain the global road shape and the motion history. Fig. 13(a) shows the result obtained at step 55. The global shape of road boundaries and the robot motion histoties from the surviving particles are shown. Colors of road boundaries indicate road types (straight, left curve, and right curve). The history obtained from odometry is also shown for comparison. Fig. 13(b) shows the result at the final step. Incorrect road models at step 55 have been eliminated and the straight shape of the road is clearly recovered.

B. Curves and Shadow

Fig. 8(b) shows the location of the second experiment. The road includes curved parts and strong shadows are cast on many locations. We obtained 180 sets of data in this case. At step 38, strong shadows are cast on the road surface (see Fig. 14(a)); this makes it difficult to detect the right road boundary using colors (see figure (d)). The intensity gradient information is not very effective, either (see figure (c)). The curbs are clearly observable in the LRF data (see figure (b)), and this make it possible to correctly estimate the road region, as shown in Fig. 15.

Figs. 16 and 17 are the input image, range and gradient information, and the estimation result at step 94. Again, a strong sunlight makes it difficult to detect road boundaries using color, but LRF data on both sides and the intensity gradient on the left are mainly used for road region estimation.

Figs. 18 and 19 are the data at step 129. Because a branch exists on the left side and a right side curb is undetectable, there is no cue for the estimation. This results in a diffision of the estimated road boundaries (see Fig. 19). A few steps later, however, the range and image data on the left side become effective to make the boundaries converge.

Fig. 20 shows the estimation results of the global road shape and the motion history at step 94 and at the final step. The approximate shape of the road is well recovered.

The number of particles certainly affect the estimation performance. We quantitatively examined their relationship for the two experimental situations. We ran the system 20 times for each number of particles and calculated the success

(a)Input image.

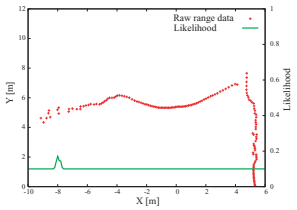

(b) Likelihood values by range data.

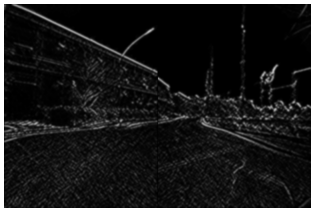

(c) Intensity gradient image.

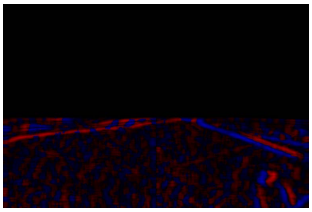

(d) Color gradient image.

Fig. 18. Observation at step 129.

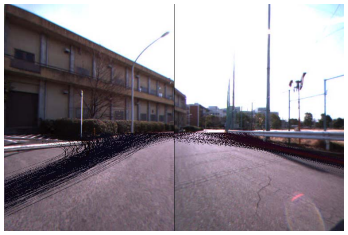

(a) Estimated road boundaries.

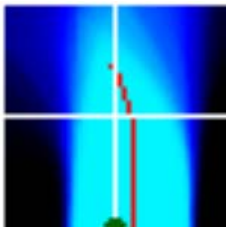

(b) Certainty distribution for road region.

Fig. 19. Estimation result at step 129

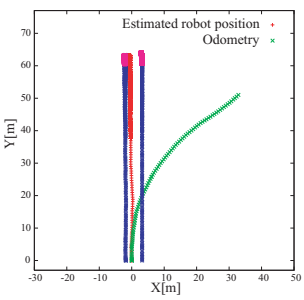

(a) Result at step 94.

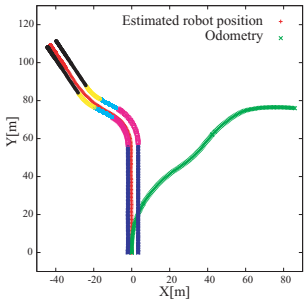

(b) Result at final step.

Fig. 20. Estimation results of global road shape.

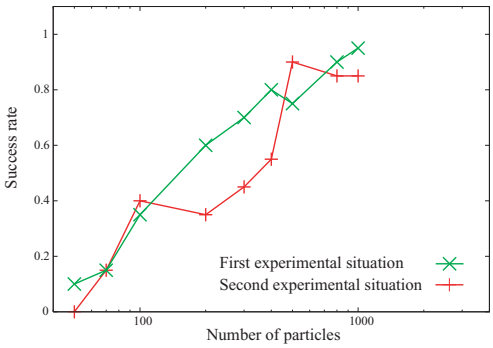

Fig. 21. Quantitative result.

Fig. 22. Autonomous driving.

rate. We judged if the estimation result is successful by visual inspection. Fig. 21 shows the result. The computation time of the proposed estimation method is about $0.5\ [sec]$ per step using 500 particles. The number of particles depends on the accuracy of dead reckoning and a model variety. Increasing the accuracy by using, for example, gyroscope, would reduce the number of particles thus reducing the computation time.

We combined the estimation method with a simple robot control procedure to perform the experiments of autonomous driving. Fig. 22 shows some snapshots of the experiments. The robot was able to robustly move autonmously in various road environments.

VII. Conclusion

This paper has described a new method of simultaneously estimating the road region and the robot ego-motion. The method effectively integrates two sources of information, vision and range finder, using a particle filter with new likelihood functions. It can also cope with the change of road types by devising a method of generating particles (hypotheses) corresponding possible road changes. The method has been tested in various real environments to show its effectiveness.

To cope with more various environments, we are planning to extend the method in the following two ways. One is to use more features to cope with various scenes. Human can recognize a road region even when no clear boundaries exist using some features which can separate road and non-road regions. Seeking and testing effective features are necessary. The other way is to add more various road models such as crossings and parking spaces where we cannot observe continuous road boundaries.

References

[1] J. D. Crisman and C. E. Thorpe. SCARF: A Color Vision System that Tracks Roads and Intersections. *IEEE Trans. on Robotics and Automation*., Vol. 9, No. 1, pp. 49-58, 1993.

[2] H. Ishiguro, K. Nishikawa, and H. Mori. Mobile Robot Navigation by Visual Sign Patterns Existing in Outdoor Environments. In *Proceedings of IEEE/RSJ Int. Conf. on Intelligent Robots and Systems*, pp. 636.641, 1992.

[3] W.S.Wijesoma, K.R.S. Kodagoda, and A.P. Balasuriya. Road Boundary Detection and Tracking Using Ladar Sensing. *IEEE Trans. on Robotics and Automation*, Vol. 20, No. 3, pp. 456-464, 2004.

[4] A. Kirchner and T. Heinrich. Model-Based Detection of Road Boundaries with a Laser Scanner. *In Proceedings of IEEE Int. Symp. on Intelligent Vehicles*, pp. 93-98, 1998.

[5] H. Cramer and G. Wanielik. Road Border Detection and Tracking in Non Cooperative Areas with a Laser Radar System. In *Proceedings of German Radar Symposium*, 2002.

[6] D. Langer and T. Jochem. Fusing Radar and Vision for Detecting, Classifying and Avoiding Roadway Obstacles. In *Proceedings of IEEE Int. Symp. on Intelligent Vehicles*, pp. 333-338, 1996.

[7] J. Miura, Y. Negishi, and Y. Shirai. Mobile Robot Map Generation by Integrating Omnidirectional Stereo and Laser Range Finder. In *Proceedings of 2002 IEEE/RSJ Int. Conf. on Intelligent Robots and Systems*, pp. 250-255, 2002.